JOURNAL OF AIRCRAFT
Vol. 45, No. 6, November–December 2008

Higher-Order Spectral Analysis of Limit Cycle Oscillations of Fighter Aircraft

Muhammad R. Hajj*
Virginia Polytechnic Institute and State University, Blacksburg, Virginia 24061
and
Philip S. Beran†
U.S. Air Force Research Laboratory, Wright–Patterson Air Force Base, Ohio 45433

DOI: 10.2514/1.34841

Higher-order spectral analysis is implemented to identify quadratic and cubic nonlinear aeroelastic phenomena associated with limit cycle oscillations encountered in a specific F-16 flight-test maneuver that consists of a straight and level flight followed by a windup turn at a Mach number near 0.95 and an altitude of 10,000 ft. The results show that nonlinear manifestations of the limit cycle oscillations are most prominent at the forward locations on the wing-tip and underwing launchers. Physical explanations of identified nonlinearities and relations to vibration modes of the different components are presented.

Introduction

FLIGHT testing of fighter aircraft/store configurations is a part of their certification for operation in flutter and limit cycle oscillation (LCO)-free envelopes. Yet the increases in numbers and combinations of store configurations and in costs associated with flight testing have made the testing of all possible configurations impractical. Consequently, different approaches have been proposed to predict onset of flutter and LCO of aircraft/store combinations. Johnson and Denegri [1] suggested mapping flight-test results into a neural network to predict LCO before other flight tests with slightly differing configurations are performed. Obviously, results from this approach would become suspect if LCO initiating conditions vary from those used in the network training. Another approach is to use numerical simulation of the aerodynamic flow and structural response as a computational tool that can be used for LCO prediction for different store configurations [2–5]. To date, the use of high-fidelity full-scale numerical simulations to predict and manage the variety of observed LCO phenomena in high-performance aircraft may be of limited value. A major reason is the significant computational power in terms of memory and speed that is required to reliably simulate the aerodynamic flow and its nonlinear interactions with rigid-body motions of the fuselage, launchers, stores, and control surfaces and grid deformation requirements to accurately communicate aerodynamic loads and structural deformations in complex configurations.

Reduced-order modeling presents an effective alternative that can be used to set up, update, make future decisions about flight-testing procedures, and predict or control LCO. The development of such models should, however, take into consideration several important issues. First, the model should be derived from equations and data that reflect all physical mechanisms. As such, deriving a reduced-order model from a numerical simulation that is not reliable enough or that does not take into account one or more of the important physical mechanisms (such as shock formation, flow separation, nonlinear structural and rigid-body motions, or coupling between different modes) may be an unproductive exercise. Second, any model should include all relevant linear and nonlinear aspects of the aerodynamic loads, the structural and rigid-body responses, the control surfaces, the interfaces of the different components, and their couplings. Finally, nonlinear behavior in flight tests can arise from unknown sources [6]. As such, developed reduced-order models should be based on identified physical phenomena from physical tests. The identification of nonlinear physical phenomena is also important for the quantification of control-surface effectiveness, the implementation of control procedures, and/or the validation of computational methodologies.

The overall goal of this effort aims at establishing the ability to conduct a robust identification of nonlinear aeroelastic behavior with the objective of enabling the development of reduced-order models for observed LCO in flight tests. Such an identification could also provide physical explanations of possible deviations from expected behaviors that are based on linear approaches. This could be the case when predictions are based on linear approaches such as μ analysis, in which it is conceivable that a nonlinear system may have a lower flutter speed than that predicted with a linear model [6]. Finally, because the identification of nonlinearities leads to a better understanding of the role of nonlinear structural, aerodynamic, and structural/aerodynamic coupling in the initiation of LCO, it can be used to provide a physics-based validation of computational tools and methodologies. In this work, higher-order spectral analysis of flight-test data is implemented to identify nonlinear aeroelastic phenomena associated with LCO encountered during flight tests of the F-16. Particular attention is given to establishing the ability to identify quadratic and cubic nonlinearities in a specific maneuver in which LCOs are encountered and that consists of a straight and level flight followed by a windup turn at a Mach number near 0.95.

Flight Testing and Analyzed Data

Flight tests for LCO on different wing/store configurations of the F-16 are conducted on a specially outfitted aircraft, administered by the U.S. Air Force's Seek Eagle program. The vehicle is instrumented with accelerometers on the wings, stores, and pylon–wing interfaces. The telemetry data are recorded by ground operators for the specific purpose of LCO identification. A strict protocol for safe LCO clearance limits has been established, and constant communication is maintained between the ground crew and the pilot during LCO testing [7]. Test procedures performed by pilots can include maneuvers such as control pulses, symmetric and antisymmetric sweeps or pulses, and windup turns. More details of these procedures are provided by Denegri [8] and Denegri et al. [9].

Presented as Paper 1797 at the 48th AIAA/ASME/ASCE/AHS/ASC Structures, Structural Dynamics, and Materials Conference, Honolulu, HI, 21–24 May 2007; received 27 September 2007; accepted for publication 24 June 2008.

*Professor, Engineering Science and Mechanics.
†Principal Research Aerospace Engineer, Air Vehicles Structural Dynamics.

Table 1 Accelerometer locations

Station	Location	ID	Inst no. (lateral, vertical)	Left side
1	Wing-tip launcher	1 (forward)	5, 6	11, 12
	BL 183	3 (aft)	2, 3	8, 9
2	Underwing launcher	4 (forward)	17, 18	23, 24
	BL 157	5 (aft)	14, 15	20, 21
2	Pylon–wing interface	6 (forward)	48, 49	52, 53
	BL 157	7 (aft)	46, 47	50, 51
3	Pylon–wing interface	8 (forward)	28, 29	32, 33
	BL 117	9 (aft)	26, 27	30, 31
4	Pylon–wing interface	10 (forward)	36, 37	40, 41
	BL 71	11 (aft)	34, 35	38, 39

The test case analyzed in this work is a maneuver test conducted at an altitude of 10,000 ft and $M = 0.95$ and is referred to as run 5. Table 1 gives identification (ID) and instrumentation (inst) numbers and locations of all accelerometers on the aircraft. Lateral and vertical accelerations as measured at ID locations 1, 4, 6, and 8, which are shown in Fig. 1, are analyzed in this work. The respective span distances of these locations from the fuselage are 183, 157, and 117 in. and will be denoted, respectively, by baseline (BL) 183, BL 157, and BL 117. The measurement range of the accelerometers was ± 10 g with a nominal sensitivity of 10 mV/g (at 100 Hz) and a noise floor of 0.0012 g (rms). The data were sampled at the rate of 325 samples/s. The case considered here corresponds to the observed typical LCO behavior as described by Denegri [8].

Higher-Order Spectral Analysis

Higher-order spectral moments are multidimensional Fourier transforms of higher-order statistics. If $x(t)$ is a real random process and its moments up to order n are stationary, one could define the nth-order moment function $m_n(\tau_1, \ldots, \tau_{n-1})$:

$$m_n(\tau_1, \ldots, \tau_{n-1}) = E\{x(t)x(t+\tau_1)\cdots x(t+\tau_{n-1})\} \tag{1}$$

where $E\{\}$ represents ensemble-averaging. Obviously, the first-order moment is the mean value. The second-order moment $E\{x(t)x(t+\tau_1)\}$ represents the autocorrelation, which is a measure of how the random process is correlated with itself at different times. The third- and fourth-order moments $E\{x(t)x(t+\tau_1)x(t+\tau_2)\}$ and $E\{x(t)x(t+\tau_1)x(t+\tau_2)x(t+\tau_3)\}$ are, respectively, referred to as the bicorrelation and tricorrelation functions.

By Fourier-transforming the preceding moment functions, one obtains the second-, third-, and fourth-order spectral moments $S_{xx}(f)$, $S_{xxx}(f_1, f_2)$, and, $S_{xxxx}(f_1, f_2, f_3)$, respectively. These quantities are referred to as the autopower spectrum, autobispectrum, and autotrispectrum. They are, respectively, expressed as

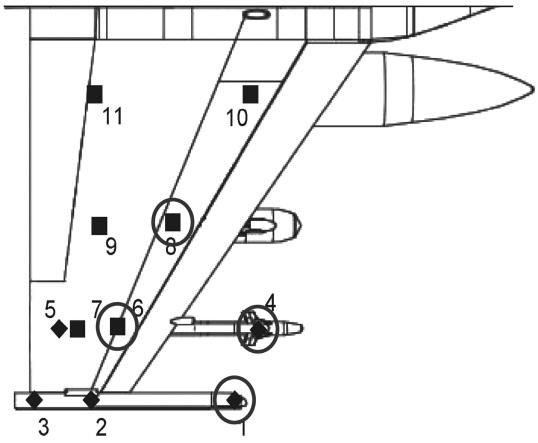

Fig. 1 Accelerometer locations used in the analysis; IDs 1, 4, 6, and 8 are indicated [9].

$$S_{xx}(f) = \lim_{T\to\infty} \frac{1}{T} E\{X^*(f)X(f)\} \tag{2}$$

$$S_{xxx}(f_1, f_2) = \lim_{T\to\infty} \frac{1}{T} E\{X^*(f_1)X^*(f_2)X(f_1+f_2)\} \tag{3}$$

and

$$S_{xxxx}(f_1, f_2, f_3) = \lim_{T\to\infty} \frac{1}{T} E\{X^*(f_1)X^*(f_2)X^*(f_3)X(f_1+f_2+f_3)\} \tag{4}$$

where $X(f)$ is the Fourier transform of $x(t)$ defined over a time duration T, and the superscript $*$ is used to denote the complex conjugate. The basis for the use of higher-order spectral analysis in the detection of nonlinear coupling among frequency modes is that if two frequency components (f_1 and f_2) and their sum components ($f_1 + f_2$) are coupled in a time series through a quadratically nonlinear interaction mechanism, phase coherence will exist among them. Under these conditions, the averaging will lead to a large value of the autobispectrum. Similarly, the cubic interaction of three frequency components (f_1, f_2, and f_3) yields a large value for the autotrispectrum.

The dependence of the autobispectrum and autotrispectrum on the amplitudes of the spectral components is removed by considering their normalized values, which, based on the Schwartz inequality, will vary between zero and one when projected onto orthogonal basis functionals. As such, the autobicoherence is defined as

$$b^2_{xxx}(f_1, f_2) = \frac{|S_{xxx}(f_1, f_2)|^2}{E\{|X(f_1+f_2)|^2\}E\{|X(f_1)X(f_2)|^2\}} \tag{5}$$

The pair of frequency components at frequencies f_1 and f_2 and their sum at $f_1 + f_2$ are then quadratically coupled if $b^2(f_1, f_2) = 1$, not quadratically coupled if $b^2(f_1, f_2) = 0$, and partially coupled if $0 < b^2(f_1, f_2) < 1$. The autotricoherence, defined as

$$t^2_{xxxx}(f_1, f_2, f_3) = \frac{|S_{xxxx}(f_1, f_2, f_3)|^2}{E\{|X(f_1+f_2+f_3)|^2\}E\{|X(f_1)X(f_2)X(f_3)|^2\}} \tag{6}$$

will also assume values between zero and one. A unit value for the autotricoherence indicates perfect cubic phase coupling, a zero value indicates no coupling, and any value between zero and one indicates partial coupling. Thus, the autotricoherence can be used to determine the extent of cubic coupling in a time series. Similar relations (cross correlations or cross coherence) can also be defined to determine quadratic and cubic coupling between frequency components from different signals. More details about these moments and their applications can be found in the work by Kim and Powers [10], Hajj et al. [11], Powers and Im [12], and Hajj et al. [13].

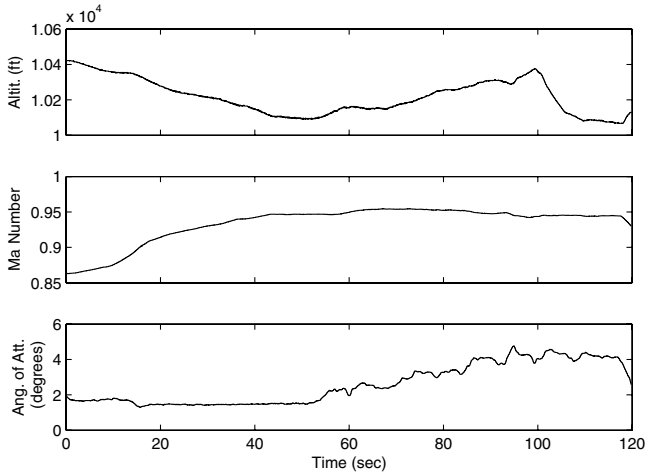

Fig. 2 Variations in altitude, Mach number, and angle of attack with time for run 5.

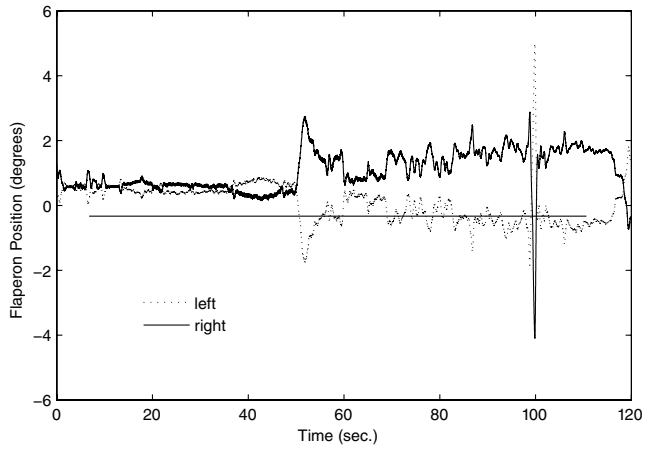

Fig. 3 Variations in the positions of the left and right flaperons for run 5.

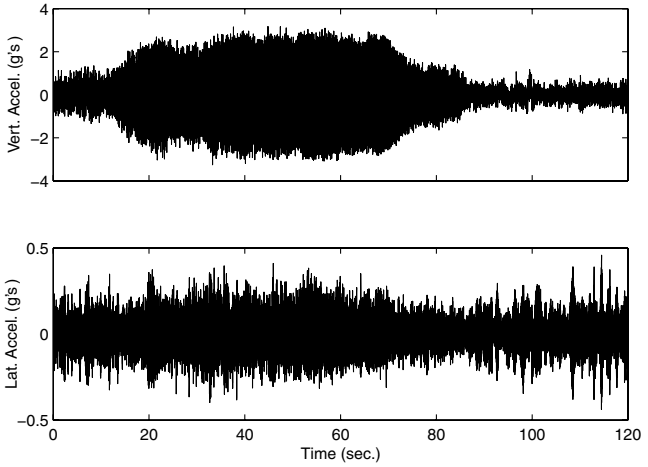

Fig. 4 Vertical and lateral accelerations as measured at the forward position of the wing-tip launcher for run 5.

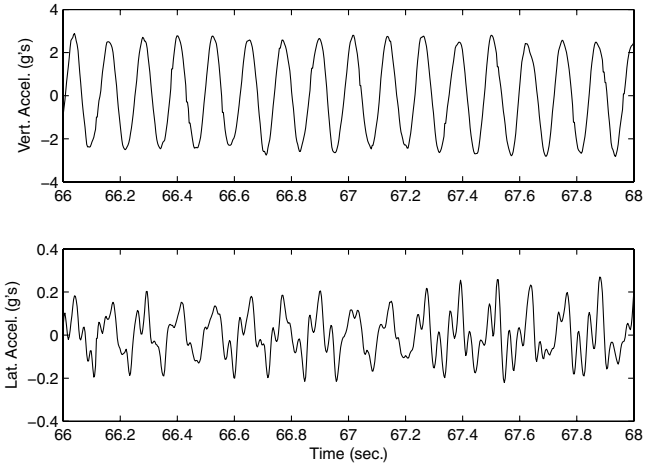

Fig. 5 Variations in the vertical and lateral accelerations at the forward position of the wing-tip launcher over a part of the record in which LCOs were encountered for run 5.

Results

Testing Conditions and Parameters

Detailed analysis of the testing parameters and measured accelerations at different locations on the aircraft in run 5 was performed. The testing parameters are presented in Fig. 2, which shows the altitude, Mach number, and angle of attack, and in Fig. 3, which shows the angular positions of the left and right flaperons. In this run, the altitude is kept constant at about 10,000 ft, and the Mach number is continuously increased from about 0.86 to 0.9 over the first 15 s and to 0.95 after about 50 s. Throughout this period, the angle of attack is maintained at a constant value near 2 deg. At approximately $t = 50$ s, a windup turn is performed by giving the flaperons opposite angular displacements, as shown in Fig. 3. Over the next 40 s, variations in the flaperon positions are introduced and the angle of attack is increased to about 4 deg. At approximately $t = 100$ s, another windup turn, whereby the flaperon positions are reversed, is performed. This reversal is most likely the control input to terminate the turn maneuver.

The measured oscillatory wing-tip accelerations during the preceding run are presented in Fig. 4. The plots show that as the Mach number is increased from 0.86 to 0.9, the amplitude of the vertical acceleration increases from approximately 0.75 to about 2 g. This level of acceleration is more or less maintained as the Mach number is increased to 0.95 and over the period when the windup turn is performed. At approximately $t = 70$ s, the amplitudes of the vertical accelerations start to decrease to reach values of about 0.4 g near $t = 100$ s. As for the lateral accelerations, it is noted that they reach a maximum amplitude of about 0.3 g and show a high level of variations in comparison with the vertical accelerations. Two-second portions of the preceding measured accelerations are shown in Fig. 5. The plots clearly show that the vertical acceleration component has one major frequency, and the horizontal component has the same component with additional harmonics.

Nonlinear Couplings in Vertical Accelerations

Power spectra of the measured vertical accelerations at the forward positions of the wing tip (ID 1, BL 183 in.), underwing launchers (ID 4, BL 157 in.), and two pylon–wing interfaces are presented in Fig. 6. The first pylon–wing interface is directly above the underwing launcher (ID 6, BL 157 in.) and the second one is further inboard (ID 8, BL 117 in.). Obviously, the major response of all components is at the frequency component near 8.2 Hz, which corresponds to the wing's antisymmetric first bending mode. The symmetric mode near 5.5 Hz has a much smaller amplitude, yet it is a part of the response at all locations. Additionally, a sharp peak near the third harmonic of the antisymmetric mode with a frequency near 24.5 Hz is also detected at all locations. The highest amplitude of this component is measured at the wing-tip and underwing launchers. On the other hand, it is much smaller at the inboard pylon–wing interface.

In cubically nonlinear systems, triplets of modes or waves with frequencies f_1, f_2, and f_3 can interact to add energy to their sum $f_4 = f_1 + f_2 + f_3$ (or difference) frequency. For the case in which $f_1 = f_2 = f_3 = f$, the cubic nonlinearity will lead to energy transfer to the third harmonic $3f$. As such, the presence of the third harmonic

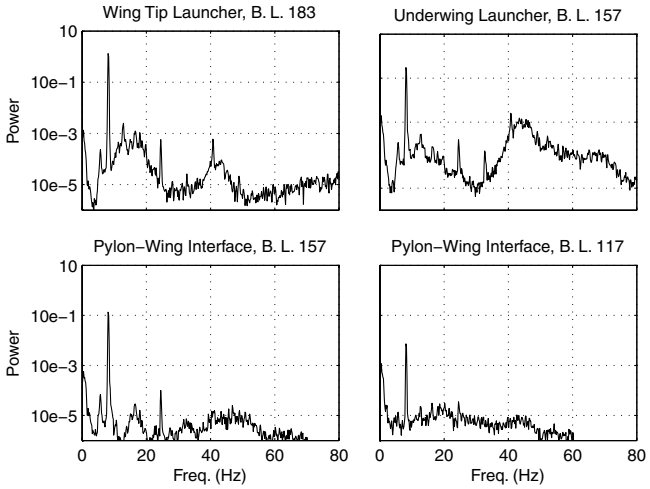

Fig. 6 Power spectra of the measured vertical accelerations at the forward positions on the specified elements for run 5.

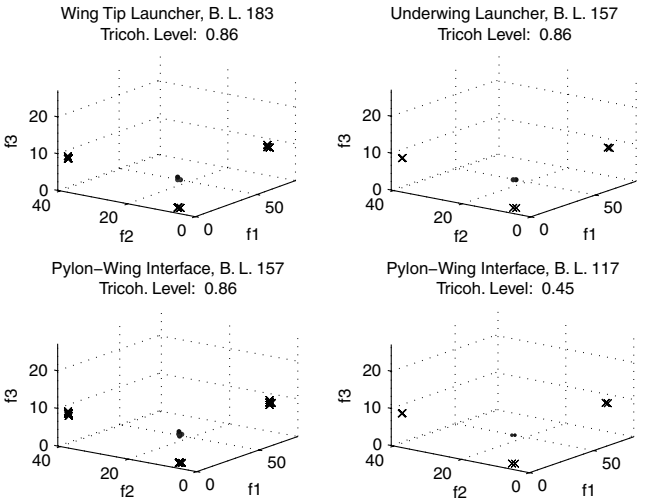

Fig. 7 Highest autotricoherence values between the different frequency components of the measured vertical accelerations at the forward positions on the specified elements for run 5.

indicates a nonlinear cubic coupling in the vertical component of the accelerations. The higher amplitude of this component at the launchers indicates a more significant nonlinear coupling at these locations and points to the source of nonlinearities that are responsible for the observed LCO. It is important to note here that the presence of a third harmonic is only an indication of the cubic nonlinearity and should not be independently used to identify or quantify the extent of a cubic nonlinearity. This can only be achieved by quantifying the extent of phase relation between the coupled modes, as would be determined from the tricoherence. When cubically coupled, the sum (or difference) mode will have a phase that is related to the phases of the interacting modes (i.e., $\theta_4 = \theta_1 + \theta_2 + \theta_3$). As explained previously, the trispectrum and its normalized value, the tricoherence, are particularly sensitive to this phase relation and could consequently be used to identify and quantify the extent of cubic nonlinearity.

The highest cubic coupling levels, as determined from the autotricoherence, between the different frequency components in the measured signals are presented in Fig. 7. As defined previously, the tricoherence is a function of three independent frequency variables, which necessitates the use of a four-dimensional space. As such, it is plotted by drawing spheres at every point in a three-dimensional frequency space. In our presentation of the tricoherence analysis results and to facilitate their interpretation, only values above a particular level are plotted, determined by a continuous decrease of the plotted levels until the first sphere appears. This yields the most relevant cubic nonlinearities. Furthermore, to enable a better reading of the figure, the spheres are projected with an "X" on the three two-dimensional planes of the plot. The results presented in Fig. 7 clearly show that the highest level of cubic nonlinear coupling is always measured between the antisymmetric mode with a frequency of 8.2 Hz and its third harmonic near 24.5 Hz. Yet this coupling level is significantly smaller (by 50%) at the inboard pylon–wing interface than at the other locations. This indicates that the source of this cubic nonlinearity is associated with the launchers. In relation to this point, one should also note the enhanced energy of the fourth and fifth harmonics in the response of the launchers, as shown by the sharp peaks near 32.7 and 41 Hz in Fig. 6. These harmonics are clearly not a part of the measured accelerations at the pylon–wing interfaces. The enhanced energy in these harmonics takes place via nonlinear couplings between the lower harmonics in the same signal or with other signals such as lateral accelerations. As such, they indicate that nonlinearities in the response of the launchers are more important than nonlinearities in the pylon–wing interface.

The levels of quadratic nonlinear coupling between the different frequency components in the measured vertical accelerations are presented in the contour plots of the autobicoherence shown in Fig. 8. The bicoherence is a function of two independent frequency variables. As such, it is plotted by drawing contour lines over a two-

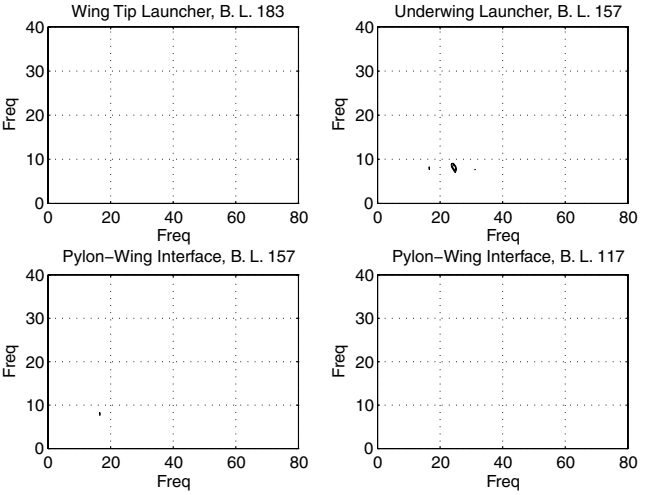

Fig. 8 Contour plots of the autobicoherence between the different frequency components of the measured vertical accelerations at the forward positions on the specified elements for run 5; contour levels are set at 0.4, 0.6, and 0.8.

dimensional frequency space. Results presented in Fig. 8 show that the levels of quadratic coupling between the different frequency components at the wing-tip launcher and wing–pylon interfaces are low (below 0.4). On the other hand, a high level of quadratic coupling (near 0.7) is estimated between the antisymmetric mode and its third harmonic in the acceleration signal of the underwing launcher. Relatively lower coupling levels (near 0.4) are noted in the same signal between the antisymmetric mode and its second and fourth harmonics. These couplings indicate that in addition to the cubic nonlinearities, the vertical component of the acceleration of the underwing launcher is characterized by quadratic nonlinearities, leading to the generation of additional harmonics observed in Fig. 6 and discussed in the previous paragraph.

In addition to the preceding, one should note the wide peaks at approximately 13 and 40 Hz in the spectra of the accelerations measured at the wing-tip and underwing launchers in Fig. 6. The 13 Hz component has a higher amplitude at the wing-tip launcher and the 40 Hz component has a higher amplitude at the underwing launcher. Because these peaks do not appear in the spectra of the accelerations of the wing–pylon interface, one can conclude that they should be associated with the motions of the wing-tip and underwing launchers. Based on ground-vibration tests of slightly different configurations, it is presumed that the peak near 13 Hz is most likely

associated with the frequency of the tip-launcher pitch and the peak near the 40 Hz component is associated with the missile's vertical bending mode. The fact that no nonlinear couplings are measured between these and other frequency components indicates that they do not contribute to the observed LCO.

Detailed analysis of the nonlinear coupling levels at the other measuring locations of the vertical accelerations, including the aft of the wing-tip-launcher location (inst 3), the aft of the underwing launcher (inst 15) and at the pylon–wing interfaces at BL 157 (aft with inst 47), BL 117 (aft with inst 27), and BL 71 (forward and aft locations (inst 37 and 35) was also performed. The results show tricoherence coupling levels of about 0.6 between the major frequency component and its third harmonic at the middle and aft of the wing-tip launcher. At all other locations, the tricoherence levels between these components were below 0.35.

Nonlinear Couplings in Lateral Accelerations

Figure 9 shows the power spectra of the measured lateral accelerations at the same positions considered in Fig. 6. Again, the major frequency component in all responses is near 8.2 Hz, which corresponds to the wing's antisymmetric first bending mode with the highest response measured at the underwing launcher station. The response amplitudes at the pylon–wing interfaces are significantly lower. Also note the fact that the clear harmonics (with sharp peaks) of this component are only present in the acceleration signals of the launchers. This indicates that the nonlinearities are more pronounced at the launchers than at the pylon–wing interfaces.

Figure 10 shows the highest cubic coupling levels, as determined from the autotricoherence, between the different frequency components in the measured lateral accelerations. The results show that cubic couplings between the major response frequency (antisymmetric mode) and its third harmonic is the highest only at the tip-launcher station. At the underwing station, the highest coupling levels are between the major frequency component and its second and third harmonics, which enables the generation of the higher-order harmonics observed in the corresponding power spectra presented in Fig. 6. At the pylon–wing interfaces, the auto-tricoherence levels are below 0.35, which indicates no cubic coupling levels at these stations.

Contour plots of the autobicoherence, indicating the level of quadratic coupling among the different frequency components in the lateral accelerations, are presented in Fig. 11. The results clearly show that the only significant quadratic couplings take place at the wing-tip launcher between the major frequency component and its second- and third-order harmonics and at the underwing launcher between the major frequency component and its harmonics (up to the sixth order) and between the second- and higher-order harmonics. These couplings explain the presence of the harmonics in the corresponding spectrum shown in Fig. 6.

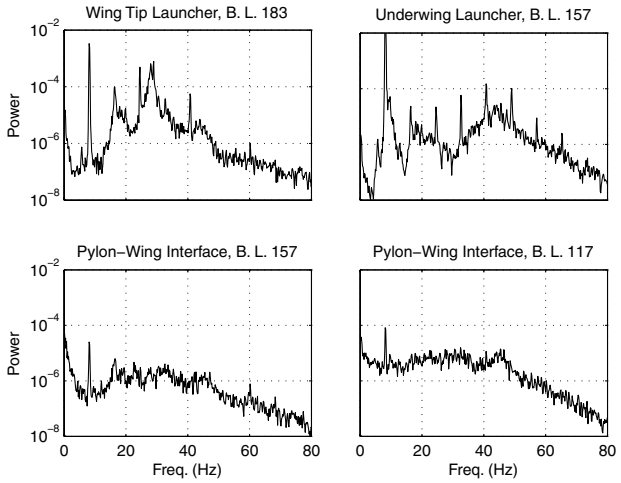

Fig. 9 Power spectra of the measured lateral accelerations at the forward positions on the specified elements for run 5.

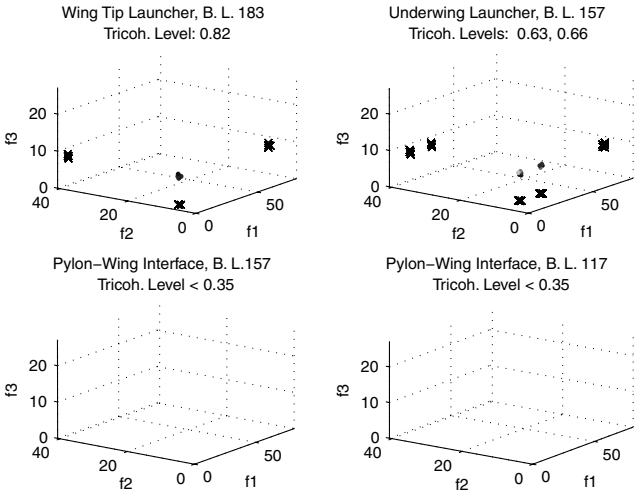

Fig. 10 Highest autotricoherence values between the different frequency components of the measured lateral accelerations at the forward positions on the specified elements for run 5.

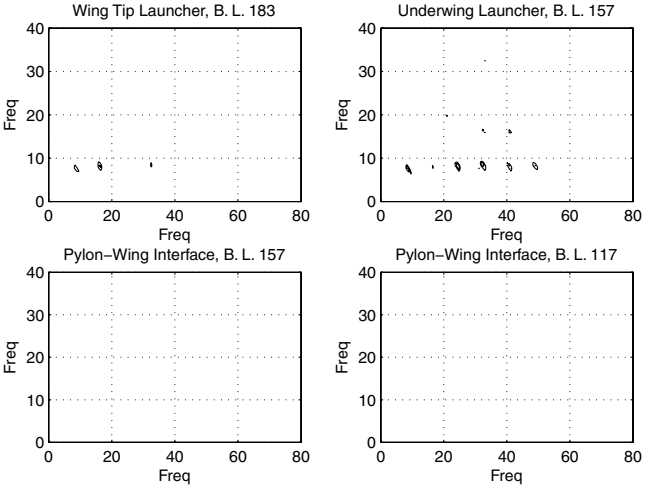

Fig. 11 Contour plots of the autobicoherence between the different frequency components of the measured lateral accelerations at the forward positions on the specified elements for run 5; contour levels are set at 0.4, 0.6, and 0.8.

Detailed analysis of the nonlinear coupling levels at the other measuring locations of the lateral accelerations, including middle and aft of the wing-tip-launcher location (inst 42 and 2), at the aft of the underwing launcher (inst 14) and at the pylon–wing interfaces at BL 157 (aft with inst 46), BL 117 (aft with inst 26), and BL 71 (forward and aft locations with inst 36 and 34) was performed. A summary of the tricoherence levels between the first antisymmetric mode and its third harmonic in measured (vertical and lateral) accelerations at the different locations on the wing and launchers is presented in Fig. 12. The results show that high tricoherence levels are measured at the forward positions of the wing-tip and underwing launchers, indicating strong cubic nonlinearities in the motions. At all other locations, tricoherence levels between the major frequency component and its third harmonic were low. Bicoherence estimates at these same locations were also below 0.4 for all frequency components. These low tricoherence and bicoherence levels indicate no important nonlinear couplings in the lateral accelerations at these locations.

Couplings Between Lateral and Vertical Accelerations at Forward Locations

The linear coherence between the same frequency components in the lateral and vertical accelerations at the same locations considered

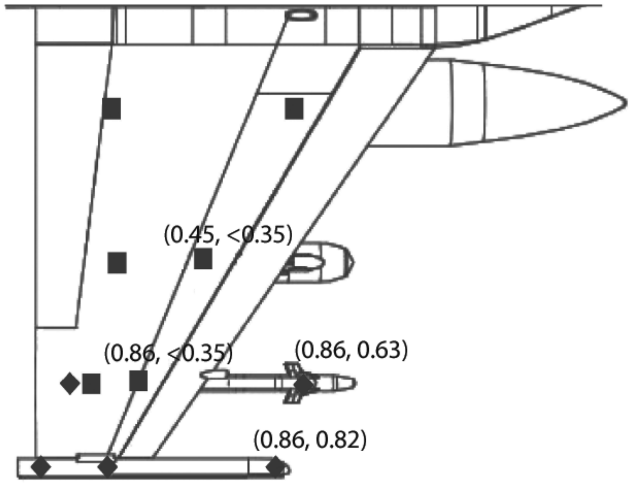

Fig. 12 Tricoherence levels between the first antisymmetric mode and its third harmonic in measured (vertical and lateral) accelerations at the different locations on the wing and launchers; low tricoherence levels (below 0.3) indicate no important cubic coupling and are therefore not overlaid on the wing schematic.

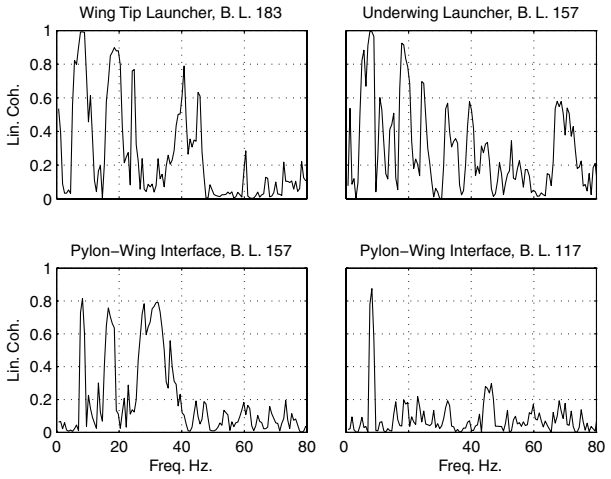

Fig. 13 Linear coherence between the same frequency components of the measured lateral and vertical accelerations at the forward positions on the specified elements for run 5.

previously are presented in Fig. 13. The results show a high degree of coupling at all locations of the major frequency component at 8.2 Hz. On the other hand, the coherence levels of the second harmonic are high at the wing-tip and underwing launchers and at the pylon–wing interface directly above the underwing launcher. This coherence level is significantly lower at the inboard pylon–wing interface. As for the third harmonic, the coherence level is high only at the launchers. On the other hand, this level is much lower at the pylon–wing interfaces. The lower coherence levels of the second and third harmonics on the pylon–wing interfaces can be related to the fact that these modes have low energy in either of the two signals, as shown in the power spectra presented in Figs. 6 and 9.

Nonlinear cross coupling between different modes in the vertical and lateral acceleration components are determined from the cross-bicoherence contour plots presented in Fig. 14. At the wing-tip launcher, high coupling is detected between the major frequency component near 8.2 Hz in the vertical response and its second harmonic near 16 Hz in the lateral acceleration. High coupling is also detected between the major frequency component near 8.2 Hz and its third harmonic near 24.5 Hz in the vertical component and their difference component near 16 Hz, which is the second harmonic, in the lateral acceleration. These results show quadratic coupling between different frequency components in the vertical acceleration

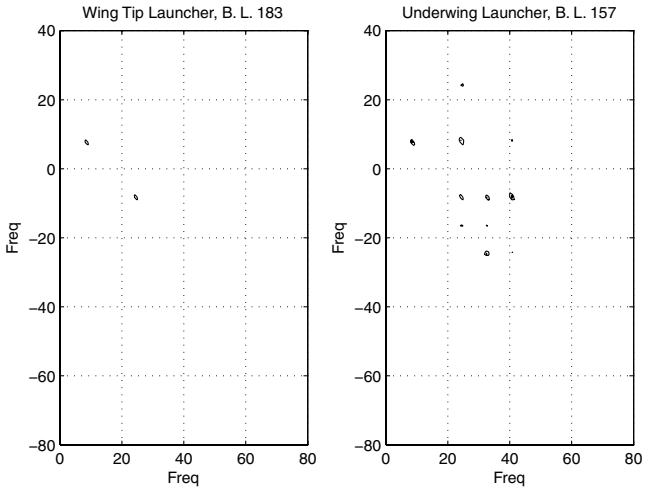

Fig. 14 Contour plots of the cross bicoherence between the different frequency components of the measured lateral and vertical accelerations at the forward positions on the specified elements for run 5; contour levels are set at 0.4, 0.6, and 0.8.

with their algebraic sum in the lateral acceleration. The second plot in Fig. 14 shows the same type of sum and difference couplings between frequency components in the vertical and lateral accelerations. Additional couplings that involve other harmonics are also present.

In summary, the results presented previously show high levels of cubic nonlinear coupling between the antisymmetric first bending mode with a frequency of 8.2 Hz and its third harmonic near 24.5 Hz in the vertical acceleration components at the forward and middle locations on the wing-tip launcher, at the forward locations of the underwing launcher, and at the forward accelerometer on the pylon–wing interface above this launcher. No other cubic nonlinear couplings were detected at any other measuring locations. No significant quadratic couplings were detected in the vertical acceleration, except at the forward location of the underwing launcher. As for the lateral accelerations, cubic nonlinear couplings were detected only at the forward location of the wing-tip launcher. Strong quadratic couplings were detected at the wing-tip launcher between the major frequency component and its second- and third-order harmonics and at the underwing launcher between the major frequency component and its harmonics (up to the sixth order) and between the second- and higher-order harmonics.

Conclusions

In this work, higher-order spectral analysis is performed to identify nonlinear aeroelastic phenomena that are associated with LCO encountered in a specific F-16 flight test. The results show that nonlinearities associated with LCO are most observable at the forward locations on the wing-tip and underwing launchers. In the vertical direction, the nonlinearity is cubic and leads to the generation of a third harmonic component. In the lateral direction, the nonlinearity is quadratic and leads to the generation of the second- and higher-order harmonics. Cross coupling between the major frequency in the vertical acceleration component and its second harmonic in the lateral acceleration is also detected. The fact that the nonlinearities were detected in the launchers and not at the pylon–wing interface indicates that they are associated with the launchers. Based on previous results regarding the effects of changing the aerodynamic shape of the launcher on the LCO [14], one could assume that the nonlinear source is actually aerodynamic and causes a flow pattern whereby the aerodynamic load yields forcing terms that are cubic in the vertical direction and quadratic in the lateral direction. This is further confirmed by the recent analysis and results of Nayfeh et al. [15], which showed that nonlinearities associated with LCO in F-16 flight tests are related to variations in the aerodynamic conditions.

References

[1] Johnson, M. R., and Denegri, C. M., "Comparison of Static and Dynamic Neural Networks for Limit Cycle Oscillation Prediction," *Journal of Aircraft*, Vol. 40, No. 1, 2003, pp. 194–203. doi:10.2514/2.3075

[2] Melville, R., "Nonlinear Mechanisms of Aeroelastic Instability for the F-16," 40th AIAA Aerospace Sciences Meeting and Exhibit, AIAA Paper 2002-0871, Reno, NV, 2002.

[3] Denegri, C. M., and Dubben, J. A., "F-16 Limit Cycle Oscillation Analysis Using Transonic Small-disturbance Theory," 46th AIAA/ASME/ASCE/AHS/ASC Structures, Structural Dynamics and Materials (SDM) Conference, AIAA Paper 2005-2296, Austin, TX, 2005.

[4] Parker, G. H., Maple, R. C., and Beran, P. S., "Analysis of Store Effects on Limit-Cycle Oscillation," 47th AIAA/ASME/ASCE/AHS/ASC Structures, Structural Dynamics and Materials (SDM) Conference, AIAA Paper 2006-1846, Newport, RI, 2006.

[5] Thomas, J. P., Dowell, E. H., Hall, K. C., and Denegri, C. M., "Virtual Aeroelastic Flight Testing for the F-16 Fighter with Stores," AIAA 2007-1640, 2007.

[6] Silva, W., Brenner, M., Cooper, J., Dengri, C., Dunn, S., Hatsell, L., Kaynes, I., Lind, R., Poirel, D., and Yurkovich, R., "Advanced Flutter and LCO Prediction Tools for Flight Test Risk and Cost Reduction–An International Collaborative Program for T & E Support," AIAA Paper 2005-7630, Dec. 2005.

[7] Dreyer, C. A., and Shoch, D. L., "F-16 Flutter Testing at Eglin Air Force Base," AIAA Paper 1986-9819, 1986.

[8] Denegri, C. M., "Limit Cycle Oscillation Flight Test Results of a Fighter with External Stores," *Journal of Aircraft*, Vol. 37, No. 5, 2000, pp. 761–769. doi:10.2514/2.2696

[9] Denegri, C. M., Dubben, J. A., and Maxwell, D. L., "In-Flight Wing Deformation Characteristics During Limit Cycle Oscillations," *Journal of Aircraft*, Vol. 42, No. 2, 2005, pp. 500–508. doi:10.2514/1.1345

[10] Kim, Y. C., and Powers, E. J., "Digital Bispectral Analysis and its Applications to Nonlinear Wave Interactions," *IEEE Transactions on Plasma Science*, Vol. 7, No. 2, 1979, pp. 120–131. doi:10.1109/TPS.1979.4317207

[11] Hajj, M. R., Miksad, R. W., and Powers, E. J., "Fundamental-Subharmonic Interaction: Effect of Phase Relation," *Journal of Fluid Mechanics*, Vol. 256, 1993, pp. 403–426. doi:10.1017/S0022112093002824

[12] Powers, E. J., and Im, S., "Introduction to Higher-Order Statistical Signal Processing and Its Applications," *Higher-Order Statistical Signal Processing*, Longman Cheshire, Melbourne, Australia, 1995.

[13] Hajj, M. R., Miksad, R. W., and Powers, E. J., "Perspective: Measurements and Analyses of Nonlinear Wave Interactions with Higher-Order Spectral Moments," *Journal of Fluids Engineering*, Vol. 119, No. 1, 1997, pp. 3–13. doi:10.1115/1.2819116

[14] Cunningham, A. M., "The Role of Non-Linear Aerodynamics in Fluid-Structure Interaction," AIAA Fluid Dynamic Conference, AIAA Paper 1998-2423, Albuquerque, NM, June 1998.

[15] Nayfeh, A. H., Hajj, M. R., Nayfeh, S. A., Chabalko, C. C., and Beran, P. S., "A Reduced-Order Model for LCO Dependence on Mach Number in F16 Flight Tests," 49th AIAA/ASME/ASCE/AHS/ASC Structures, Structural Dynamics, and Materials Conference, AIAA Paper 2008-1755, Schaumburg, IL, Apr. 2008.